AIP | Physics of Plasmas
#1 JOURNAL IN 2014 GOOGLE SCHOLAR METRICS FOR THE PLASMA & FUSION CATEGORY

Suppression of turbulent resistivity in turbulent Couette flow

Jiahe Si, Stirling A. Colgate, Richard G. Sonnenfeld, Mark D. Nornberg, Hui Li, Arthur S. Colgate, David J. Westpfahl , Jr., Van D. Romero, and Joe Martinic

Citation: Physics of Plasmas **22**, 072304 (2015); doi: 10.1063/1.4926582
View online: http://dx.doi.org/10.1063/1.4926582
View Table of Contents: http://scitation.aip.org/content/aip/journal/pop/22/7?ver=pdfcov
Published by the AIP Publishing

PHYSICS OF PLASMAS **22**, 072304 (2015)

Suppression of turbulent resistivity in turbulent Couette flow

Jiahe Si,[1,a)] Stirling A. Colgate,[2,b)] Richard G. Sonnenfeld,[1] Mark D. Nornberg,[3] Hui Li,[2] Arthur S. Colgate,[1] David J. Westpfahl, Jr.,[1] Van D. Romero,[1] and Joe Martinic[1]
[1]*New Mexico Institute of Mining and Technology, Socorro, New Mexico 87801, USA*
[2]*Los Alamos National Laboratory, Los Alamos, New Mexico 87544, USA*
[3]*University of Wisconsin-Madison, Madison, Wisconsin 53706, USA*

(Received 28 April 2015; accepted 25 June 2015; published online 13 July 2015)

Turbulent transport in rapidly rotating shear flow very efficiently transports angular momentum, a critical feature of instabilities responsible both for the dynamics of accretion disks and the turbulent power dissipation in a centrifuge. Turbulent mixing can efficiently transport other quantities like heat and even magnetic flux by enhanced diffusion. This enhancement is particularly evident in homogeneous, isotropic turbulent flows of liquid metals. In the New Mexico dynamo experiment, the effective resistivity is measured using both differential rotation and pulsed magnetic field decay to demonstrate that at very high Reynolds number rotating shear flow can be described entirely by mean flow induction with very little contribution from correlated velocity fluctuations. © *2015 AIP Publishing LLC*. [http://dx.doi.org/10.1063/1.4926582]

I. INTRODUCTION

Magnetic fields play a very important role in diverse astrophysical phenomena such as the earth's magnetic field, the dynamics of stellar atmospheres, pulsars, and active galactic nuclei.[1–4] Despite their importance, the origin of astrophysical magnetic fields is not fully understood.

A widely held concept in astrophysics is that the magnetic energy of the universe arises from the conversion of kinetic energy of motion of ionized gas flows through an electromagnetic inductive process known as the dynamo effect. The dynamo effect requires very weak "seed" magnetic fields which are then amplified by induction in conducting flows.

Recently, dynamo action has been demonstrated by a small number of laboratory experiments: The Riga dynamo experiment produced a Ponomarenko dynamo;[5–8] the Karlsruhe dynamo experiment demonstrated a homogeneous two-scale dynamo;[9,10] and the Von Karman Sodium dynamo experiment at Cadarache have demonstrated that magnetic field can be generated by a turbulent flow of liquid sodium.[11–13] However, a direct analog of an astronomical dynamo has yet to be demonstrated.

The dynamics of dynamo actions are governed by the magnetic induction equation

$$\frac{\partial \mathbf{B}}{\partial t} = \nabla \times (\mathbf{u} \times \mathbf{B}) + \frac{\eta}{\mu_0}\nabla^2 \mathbf{B}, \tag{1}$$

where $\mathbf{B}$, $\mathbf{u}$, and η are magnetic field, flow velocity, and resistivity, respectively. Large scale semi-laminar flows (we will call these *coherent* flows) may certainly induce dynamo effects.[14–19] However, a key component of most dynamo theories concerns turbulent flows. Specifically, it is supposed that a mean turbulent electromotive force ε can be generated from correlated portions of flow velocity fluctuations $\tilde{\mathbf{u}}$ and magnetic field fluctuations $\tilde{\mathbf{B}}$,[20,21] i.e.,

$$\varepsilon = \langle \tilde{\mathbf{u}} \times \tilde{\mathbf{B}} \rangle, \tag{2}$$

where the $\langle\rangle$ indicates an appropriate ensemble average. In the kinematic regime (when the effect of Lorentz force on the flow field is negligible), $\tilde{\mathbf{B}}$ can be determined from $\bar{\mathbf{B}}$, $\bar{\mathbf{u}}$, and $\tilde{\mathbf{u}}$. Retaining only first order derivatives of $\mathbf{B}$ (sometimes called "first order smoothing"[22]), Eq. (2) becomes

$$\varepsilon_{ij} = \alpha_{ij}\bar{B}_j + \beta_{ijk}\frac{\partial \bar{B}_j}{x_k}, \tag{3}$$

where α_{ij} and β_{ijk} are tensors depending on $\bar{\mathbf{u}}$, $\tilde{\mathbf{u}}$, and $\bar{\mathbf{B}}$.

The details of velocity fluctuations due to particular hydrodynamic instabilities are difficult to know *a priori*, so it is common to assume that they are isotropic and homogeneous. In this idealized framework, the tensor β_{ijk} is reduced to a scalar β. In this approximation, Krause and Rädler obtained[20]

$$\beta \approx \tilde{u}^2 \tau_{cor}/3, \tag{4}$$

where τ_{cor} is the correlation time of $\tilde{\mathbf{u}}$. Substitution of the α and β transport coefficients back into Eq. (1) reveals that the velocity correlations contribute to an enhancement of the magnetic diffusivity so that $\eta \rightarrow \eta + \mu_0\beta$.[23–25]

In the Wisconsin liquid sodium dynamo, the turbulent flows within are well approximated as homogeneous and isotropic.[26] Rahbarnia *et al.*[27] measured that the magnetic diffusive term accounts for the majority of the directly measured turbulent emf ε.

The New Mexico dynamo experiment utilizes Taylor-Couette flow between two cylinders to provide sufficient differential rotation for magnetic field amplification.[15,16,19] Operation in the hydrodynamically unstable regime makes it capable of studying turbulence superposed on a rapidly rotating flow field. Turbulent flows are generated merely by

a)Electronic mail: jsi@nmt.edu
b)Deceased.

spinning the inner cylinder while keeping the outer one at rest. The detailed experimental setup is described in Sec. II.

In this paper, we report a series of experiments conducted to study turbulent magnetic diffusivity in an unstable Taylor-Couette flow of liquid sodium. Estimates of the turbulent intensity from observed torque scalings show that the inductive response of the turbulent fluid to an applied magnetic field should show saturation of the induced azimuthal magnetic field (Sec. III A) and the decay time of a pulsed magnetic field should be shortened with respect to the resistive decay time of sodium (Sec. III B) for turbulence that is homogenous, isotropic, and has a correlation length comparable to the radial gap. The rotation rates at which turbulent dissipation is expected to affect the inductive response to applied magnetic fields is well within the range of rotation rates studied, and yet the data from both of these induction measurements show that the effects of turbulence are minimal at high rotation rate. At lower rotation rate, some amount of gain saturation is observed, but the trend at large rotation is consistent with negligible effective turbulent resistivity. Fluctuation measurements of both the magnetic field and the pressure suggest that the correlation time is changing with rotation rate which may be why the turbulent resistivity is suppressed.

II. THE NEW MEXICO DYNAMO EXPERIMENT AND DIAGNOSTICS

Taylor-Couette flow is generated in the left part of the apparatus, as shown in Fig. 1, between two co-axial cylinders with a radius ratio of $R_{\rm in}/R_{\rm out} = 0.5$ ($R_{\rm in} = 15.2$ cm and $R_{\rm out} = 30.5$ cm). With this radius ratio, the typical shear scale length is $\Delta R = R_{\rm out} - R_{\rm in} = 15.2$ cm. The length of the inner cylinder L is 30.5 cm, hence the aspect ratio $\Gamma = L/\Delta R = 2$. The end-plates rotate with the outer cylinder.

Quasi-laminar (low turbulent), nearly stable Couette flows can be generated with two cylinders spinning with angular velocity ratio $\Omega_{in} : \Omega_{\rm out} \approx 4 : 1$. At $\Omega_{in}/2\pi = 68$ Hz and $\Omega_{out}/2\pi = 17.5$ Hz, we have observed that the induced toroidal field is about 8 times of the externally applied poloidal field in the mid-plane.[19] In the right side of the apparatus a piston is being developed to drive plumes into the shear flow. These plumes inject helicity that will complete the positive feedback loop for an $\alpha\omega$ dynamo.[19,28,29]

The two co-axial cylinders are driven by a 50 horsepower (37 kW) AC motor rotating at a roughly constant 1760 rpm. The speed of the inner cylinder is varied from this fixed motor speed by two manual truck transmissions arranged in series. An arrangement of belts and gears allows the outer cylinder to be driven at a fixed fraction (typically 1/4) of the inner cylinder rotation rate. However, in this set of experiments, the outer cylinder was held stationary by a fixed torque arm. A force sensor measures the torque due to turbulent transport of angular momentum (Measurement Specialties FX1901-0001-50L).

Two temperature sensors (Honeywell® TMP36) mounted on each end-plate provide temperature measurements used to estimate the viscosity and resistivity of the working fluids.

Two magnetic coils with 20 turns each are arranged in an approximate Helmholtz configuration to provide a test field for measuring advection and diffusion of magnetic flux. The coil currents are reversible so that test fields that are predominantly either dipole or quadrupole can be generated. When the currents are in parallel, the generated dipole field is pointing from north to south (from left to right in Fig. 1). When the currents are opposite, the radial field in the mid-plane is pointing outward.

An array of seven pressure sensors (Honeywell 40PC500G3A) are mounted on the left end-plate at r = 17.1, 19.1, 21.0, 22.9, 24.8, 26.7, and 28.6 cm. For quasi-laminar flows, as discussed in our previous publication,[14] the pressure

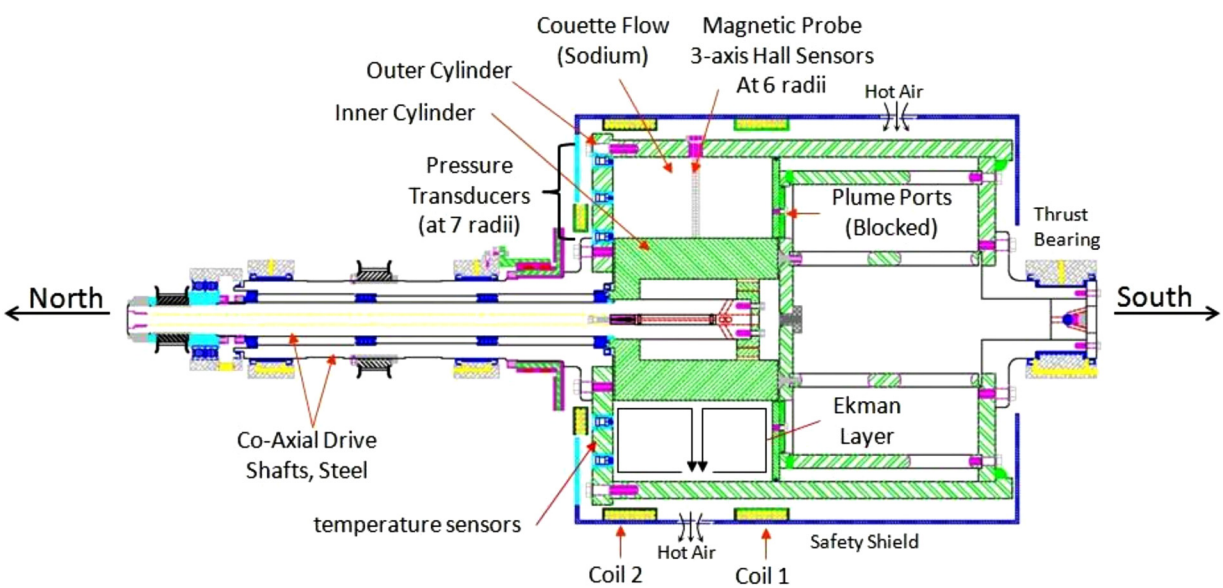

FIG. 1. Dynamo apparatus (current state): The outer cylinder is 61 cm in diameter, the inner is 30.5 cm. The apparatus is separated in two parts by a plate in the middle. The right part is for future α phase. The left part is an annulus, where a Taylor-Couette flow is created. Pressure sensors are mounted on the left end-plate at 7 radii; 2 temperature sensors are on each end-plate; a magnetic probe with 18 Hall sensors at 6 radii in 3 orthogonal directions is in the mid-plane of the annulus. National Instruments NI-8205 A/D Modules are used. National Instruments LabView is used to record and store data in the DAQ computer.

profile can be used to estimate the fluid velocity profile. But when flow is turbulent, the velocity profile cannot be easily inferred from the pressure profile. Nonetheless, the pressure fluctuation can still be used to estimate the magnitude of velocity fluctuation where $\Delta p \sim \rho \tilde{u}^2$, as discussed by Landau.[30] To boost the signal-to-noise level of the pressure fluctuation signal, $\times 200$ gain high-pass amplifiers with a cutoff frequency $f_{\text{cutoff}} = 1$ Hz are connected to the pressure sensor outputs.

A streamlined magnetic probe with 6 sets of Hall sensors in 3 cylindrical directions (Honeywell SS49E) is mounted on the mid-plane, as shown in Fig. 1. The probe is made of aluminum alloy 5083-H3 with a wall thickness of 1 mm for a cutoff frequency of about 21 kHz ($\delta = \sqrt{\eta_{Al}/\pi f \mu_0}$ with $\eta_{Al} = 8.3 \times 10^{-8}\,\Omega\,\text{m}$ at 110 °C). In this article, we focus on magnetic field fluctuations with frequency less than 400 Hz. Thus, the shielding effect of the aluminum wall on the magnetic sensors is insignificant.

Data from the sensors are sampled by National Instruments NI-9205 Analog-to-Digital Modules. LabView is used to control and receive data from the modules.

For the experiments in this work, we define the fluid and magnetic Reynolds numbers as[31]

$$\text{Re} = \frac{(\Omega_{\text{in}} - \Omega_{\text{out}})\Delta R^2}{\nu} = \frac{\Omega_{\text{in}}\Delta R^2}{\nu}, \tag{5}$$

$$\text{Rm} = \frac{(\Omega_{\text{in}} - \Omega_{\text{out}})\Delta R^2}{\eta/\mu_0} = \frac{\Omega_{\text{in}}\Delta R^2}{\eta/\mu_0}, \tag{6}$$

where the last equality applied for $\Omega_{\text{out}} = 0$. In our experiment, $Re \sim 10^6$ to 10^7. One of the advantages of making the outer cylinder stationary is that Taylor-Couette flows in this configuration have been studied extensively.[32–41]

III. METHODS USED TO STUDY THE EFFECT OF TURBULENCE

In the experiment, we used two methods to study the effects of the turbulence. The first method is to measure the amplification of an azimuthal component to the magnetic field by differential rotation (known as the ω-effect). The inner cylinder rotation rate was varied and an external *quadrupole* field (current in the two coils opposite) was applied. We define the ω-gain as the ratio of the measured mean azimuthal magnetic field $\overline{B_\theta}$ to the externally applied radial field B_{r0}, or

$$\omega\text{–gain} = \frac{\overline{B_\theta}}{B_{r0}}. \tag{7}$$

The steady-state amplitude of the azimuthal magnetic field is a balance between advection of the applied radial field and diffusion of the azimuthal field. As such, their ratio is proportional to Rm. Considering the possibility of an anisotropic effective resistivity, since the azimuthal field is generated by currents parallel to the rotation axis, the ω-gain is sensitive to changes in $\eta_{\parallel}^{\text{turb}}$ (see Sec. III A).

The second method is to measure the decay time of the axial field B_z. The speed on the inner cylinder is varied, and an external *dipole* field (current in the two coils the same direction) is abruptly shut off. The rate of decay of this field measured at the apparatus midpoint yields a second way of characterizing turbulent resistivity. We will refer to this method as the *penetration-method*, sensitive to $\eta_{\perp}^{\text{turb}}$ (see Sec. IV D).

Having introduced the two methods, we need to elaborate on the theory and measurement details to properly understand the results.

A. ω method

In a high-Re flow, the eddies in the bulk of the flow with sizes much less than the size of the apparatus can very efficiently transport angular momentum so that, on average, the specific angular momentum profile $\bar{L}_\theta(r) = \bar{\Omega} r^2$ is flat, as shown in Fig. 2. This has been observed numerically (e.g., Brauckmann and Eckhardt[41]) and experimentally (e.g., Smith,[33] Lewis,[36] and Burin *et al.*[40]) at $Re \sim 10^6$. To good approximation it is constant with radius and given by[33,36]

$$\bar{L}_\theta = \bar{\Omega}(r) r^2 = \Omega_{\text{in}} R_{\text{in}}^2/2. \tag{8}$$

This means, in our case, the mean velocity shear is proportional to Ω_{in}. If the Lorentz force and η^{turb} are negligible, the ω-gain should be proportional to the speed of the inner cylinder Ω_{in} or ω–gain $\propto$ Rm.

It should be noted that the magnetic field strength in these experiments is low enough that we can assume we are in the kinematic regime. The magnitude of magnetic energy and kinetic energy can be inferred from the relative magnitude of the Alfvén speed and the flow speed. The externally applied magnetic field is about 3 G for the quadrupole field, 6 G for the dipole field. Including the induced magnetic field, the total field is no higher than 10 G. Hence, the Alfvén speed

$$V_A = \frac{B}{\sqrt{\mu_0 \rho}}$$

is not higher than 4 cm/s, which is much smaller than the flow speed in the bulk (several tens of m/s). So the Lorentz force effect on the flow is insignificant.

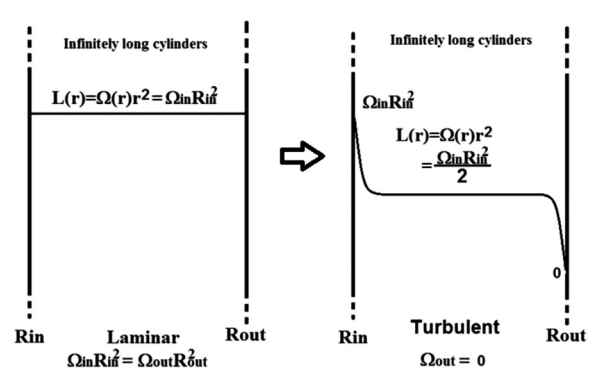

FIG. 2. Mean specific angular momentum profile. On the left, both cylinders are rotating, $\Omega_{\text{in}} R_{\text{in}}^2 = \Omega_{\text{out}} R_{\text{out}}^2$. On the right, the inner one is rotating and the outer one is at rest.

In our past publication,[19] where the ω-gain was measured in rotating shear flow, we observed that the ω-gain is about 6.4 at R = 16.3 cm, at $Rm = 92$ (for $\Omega_{\rm in}/2\pi = 68.0$ Hz and $\Omega_{\rm out}/2\pi = 17.5$ Hz at $T = 115\,^{\circ}$C). Neglecting the end-plate effect, the specific angular momentum was $L(r) = \omega_{\rm in} R_{\rm in}^2$ so that the mean velocity shear was twice as large for the same Ω_{in} with the outer cylinder stationary. Assuming that the new velocity shear when the outer cylinder is stationary is halved, based on the definition given in Eq. (6), as Ω_{out} decreases to 0, Rm should increase to 124, we would predict a gain of 3.2 at Rm = 124 at R = 16.3 cm in the absence of any additional effects from turbulence.

In a fully turbulent state, the characteristic length is limited by the gap width $\Delta R = 15.2$ cm. If we assume that the velocity fluctuations have this maximum correlation length and are homogeneous and isotropic, then the power dissipation rate per unit mass ϵ is

$$\epsilon \approx \frac{\tilde{u}^3}{\Delta R} \approx \frac{1}{2}\frac{T\Omega_{\rm in}}{\rho V}, \tag{9}$$

where T is the applied torque, ρ is the fluid density, and V is the fluid volume.[42] The factor of 1/2 comes from a paper by Lewis,[36] who found the energy dissipated by turbulence is higher in the boundary layer so that the measured dissipation in the bulk is roughly 50% of the total dissipation (ranging between 30% and 50%). From Eq. (9), we have

$$\tilde{u} \approx \left(\frac{1}{2}\frac{T\Omega_{\rm in}\Delta R}{\rho V}\right)^{1/3}. \tag{10}$$

For these large-scale velocity correlation lengths of $\tilde{u}\tau_{cor} \approx \Delta R$, the predicted turbulent enhancement of the resistivity given by Eq. (4) becomes

$$\eta^{\rm turb} \approx \mu_0 \tilde{u}\Delta R/3 \approx \frac{\mu_0}{3}\left(\frac{T\Omega_{\rm in}\Delta R^4}{2\rho V}\right)^{1/3}, \tag{11}$$

$$\approx \frac{\mu_0 \nu \Delta R}{3}\left(\frac{G\mathrm{Re}}{2\pi\left(R_{\rm out}^2 - R_{\rm in}^2\right)\Delta R}\right)^{1/3}, \tag{12}$$

where we have substituted the definition of the Reynolds number and introduced the dimensionless torque $G = T/\rho\nu^2 L$. In this form, we see that the scaling of $\eta^{\rm turb}$ with Reynolds number can be determined if we know the scaling of the required torque with Reynolds number. As shown in Section IV A, $G \propto \mathrm{Re}^2$ hence $\eta^{\rm turb}$ increases with Re. So long as the correlation length remains ΔR, the effective magnetic Reynolds number Rm no longer scales linearly with rotation rate. Rather

$$\mathrm{Rm}_{\rm eff} = \mathrm{Rm}\frac{\eta}{\eta + \eta^{\rm turb}} = \frac{\mu_0 \nu \mathrm{Re}}{\eta + \eta^{\rm turb}(\mathrm{Re})}. \tag{13}$$

We see from Eq. (13) that effective Rm at high rotation rate can be saturated by the enhanced turbulent dissipation. If the correlation length is not ΔR or if the velocity correlations are suppressed in a particular direction due to anisotropy, the turbulent dissipation rate estimated above will be too large. In this sense, Eq. (13) represents a lower bound estimate for the scaling of magnetic induction.

When anisotropic cases are considered, we note that ω-gain is mainly affected by $\eta_{\parallel}^{\rm turb}$. In the quadrupole magnetic field configuration, in the mid-plane, the major EMF is $B_r U_\theta$ along the rotation axis. So ω-gain measurement at different $\Omega_{\rm in}$'s reflects how $\eta_{\parallel}^{\rm turb}$ varies with $\Omega_{\rm in}$.

Given that we lack either a model or a measurement of the actual velocity correlation length prior to operating the experiment, our expectation is that the measured gain (and $Rm_{\rm eff}$) will lie between a curve describing the saturation effect of Eq. (13) and a linear scaling based on prior gain measurements in stable Couette flow.

B. Penetration method

When an external field outside a conductor is suddenly removed, e.g., as shown in Fig. 7, it takes time for the magnetic field to damp to zero based on the resistive diffusion of magnetic flux through the fluid. We use this property to measure the effective resistivity of the fluid by establishing an initial dipole field with the two external magnetic coils while the inner cylinder is spinning. Once B_z becomes steady, the coil currents are shut off and the decay of B_z is observed.

The resulting change in the externally applied magnetic field induces azimuthal currents in the sodium which according to Ohm's law are

$$J_\theta = \frac{E_\theta}{\eta} - \tilde{v}_r B_z - \tilde{v}_r \tilde{B}_z + \tilde{v}_z \tilde{B}_r. \tag{14}$$

Ensemble averaging will eliminate the $\tilde{v}_r B_z$ term since the velocity fluctuations are incoherent across the ensemble. Only the nonlinear turbulent emf terms will remain which we recognize as the components of ε_θ. The resulting axial component of the induction equation be

$$\frac{\partial}{\partial t}\overline{B_z} = \left(\frac{\eta}{\mu_0} + \beta_\perp\right)\nabla^2\overline{B_z} = \frac{\eta + \eta_\perp^{\rm turb}}{\mu_0}\nabla^2\overline{B_z}, \tag{15}$$

where we have neglected any contribution from the α-effect. In the Appendix, we derive the expected $B_z(t)$ for the simplified case, in which a uniform axial external field B_{z0} is suddenly removed outside an infinitely long cylinder. The analytical solution is

$$\overline{B_z}(t,r) = \sum_{n=1}^{\infty}\frac{2B_0}{k_n J_1(k_n)} J_0(k_n r/R_0)\exp\left(-\frac{\eta + \eta_\perp^{\rm turb}}{\mu_0}\frac{k_n^2}{R_0^2}t\right), \tag{16}$$

where J_1 and J_0 are the Bessel function of the first kind, first and zeroth order, respectively, k_n are the zeros of J_0, and $\eta_\perp$ is the effective resistivity perpendicular to the axis of rotation.

Since we are working in a finite cylinder, this model will be inadequate to describe the time-varying profile of the axial magnetic field. We can, however, look for variations in the decay time of the measured magnetic field for evidence

of an enhancement of the resistive decay by turbulent diffusion.

IV. EXPERIMENTAL RESULTS AND DISCUSSION

A. Torque measurement with water and turbulent resistivity estimate

The scaling of the dimensionless torque $G = T/\rho\nu^2 L$ with Re is a much-studied aspect of turbulent dissipation in Taylor-Couette flow. The dimensionless torque follows a power-law scaling when the outer cylinder is stationary, i.e., $G \propto \mathrm{Re}^{\alpha}$, where α depends on Re. As Re increases, α increases from about 1.5 (for $\mathrm{Re}_c < \mathrm{Re} < 800$)[37] to 1.87 (for $\mathrm{Re} \sim 10^6$).[35] Our measurement shows that $\alpha = 2$ for $\mathrm{Re} \geq 4 \times 10^6$, as shown in Fig. 3. This observation is consistent with the derivation by Lathrop,[35] Doering,[43] and Eckhardt[39] that also arrives at an upper bound of $\alpha = 2$.

We can use the measured dimensionless torque in Fig. 3 to estimate the expected η^{turb} by using Eq. (12). The power dissipation per unit mass ϵ is estimated by Eq. (9), where the mass of the water is 68 kg. Sodium has a similar density and kinematic viscosity to water and so the results should apply to the MHD experiments as well. Using $G \propto \mathrm{Re}^2$, we find from Eq. (13) that

$$\eta^{\mathrm{turb}} \approx \frac{\mu_0 \nu \Delta R}{3}\left(\frac{CRe^3}{2\pi\left(R_{\mathrm{out}}^2 - R_{\mathrm{in}}^2\right)\Delta R}\right)^{1/3} = \kappa \mathrm{Re}, \tag{17}$$

where $G = C\mathrm{Re}^2$, and $C = 6.5 \times 10^{-3}$, $\kappa = 2.02 \times 10^{-14}\,\Omega \cdot \mathrm{m}$ are determined from the torque measurements. Consequently, from Eq. (13), we have

$$\mathrm{Rm}_{\mathrm{eff}} = \frac{\mu_0 \nu \mathrm{Re}}{\eta + \kappa \mathrm{Re}} \tag{18}$$

from which we can infer that as $\mathrm{Re} \to \infty$, $\mathrm{Rm}_{\mathrm{eff}}$ saturates to a value of $\mu_0 \nu/\kappa \approx 46$. We find that the turbulent enhancement to resistive diffusion should be comparable to that of the sodium resistivity at a Reynolds number of $Re = \eta/\kappa \approx 5 \times 10^6$ or a rotation rate of about 25 Hz.

If our assumptions about the velocity correlations (maximum length, homogeneity, and isotropy) are valid, ω-gain saturation should be observed in our experiment.

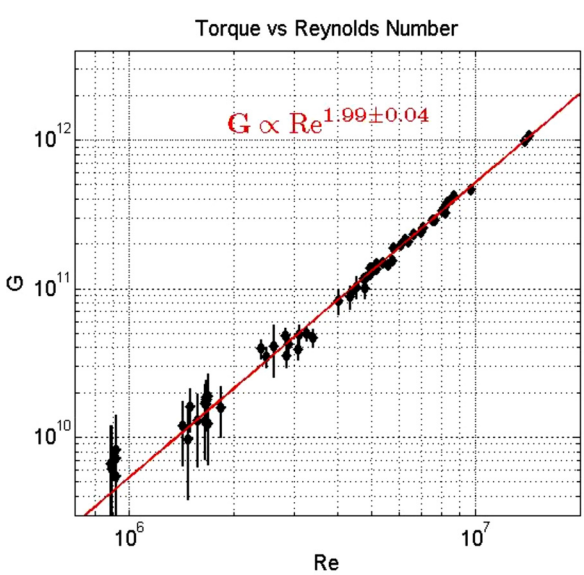

FIG. 3. Non-dimensional Torque $G = T/\rho\nu^2 L$ vs Re, where T is torque, ρ is density, ν is kinematic viscosity, and L is the length of the Taylor-Couette annulus. Data points with $\mathrm{Re} \geq 4 \times 10^6$ are used for the linear curve fitting.

B. ω-gain measurement

Measurements of ω-gain as a function of Rm are shown in Fig. 4. Five dotted lines are shown in the figure to guide the eye. For the outermost position (R = 26.5 cm, 1.5 cm away from the wall of the outer cylinder), the four measurements of ω-gain fall roughly on the same line. However, for smaller radii, there is a clear transition around Rm = 31.

Figure 5 shows the gain measurements for the innermost sensor location along with the expected scaling for the cases with and without the effects of a turbulent resistivity, as described in Sec. III A. Precise numerical agreement between the data and the curves shown is not expected since the arguments in Sec. III A treat a highly idealized problem of an infinite cylinder and neglects advection effects due to Ekman circulation. Nevertheless, the comparison of the data with the two curves in Fig. 5 illustrates: (1) there is a broad range of anticipated experimental outcomes depending on assumptions about the velocity statistics; (2) at low rotation rates, there is indication of apparent saturation of the ω-gain due to turbulent fluctuations; and (3) there is a transition at higher rotation rate to a linear dependence on cylinder rotation rate. According to our discussion, if $\eta^{\mathrm{turb}} \ll \eta_{Na}$, the dynamo gain increases linearly with Rm which we observe for the highest two rotation rates. Therefore, the turbulent enhancement to resistive diffusion parallel to the rotation axis is small compared with the sodium resistivity at high Reynolds number.

C. Fluctuation spectra and correlation times

Lacking a diagnostic to specifically measure the mean velocity and velocity fluctuations, we can infer information about the velocity fluctuations through measurements of the magnetic field and pressure fluctuation spectra. We have observed coherent behavior at low rotation rates, which vanishes at higher rotation rates. This suggests that the coherence length of the velocity fluctuations is decreasing at higher rotation rates. Supporting evidence for this conclusion is presented in the rest of this section.

From Figs. 6(a) and 6(b), it can be seen that at the lower rotation rates, both spectra show a strong low frequency peak that disappears at higher rotation rate. At an inner cylinder rotation rate of $f_{\mathrm{in}} = 9.3$ Hz, we have observed a prominent peak in B_θ at $0.29\, f/f_{\mathrm{in}}$ (red curve). As the rotation rate is increased to $f_{\mathrm{in}} = 17.1$ Hz, this peak persists at a very similar frequency ratio $0.26\, f/f_{\mathrm{in}}$. However, as we move to higher rotation rates of 28.8 and 47.6 Hz, the characteristic frequency vanishes. Furthermore, this same frequency is observed at all radii measured (A prominent peak was not observed at the outermost sensor at f_{in}=9.3 Hz. Its absence is likely due to very low (0.18) ω-gain).

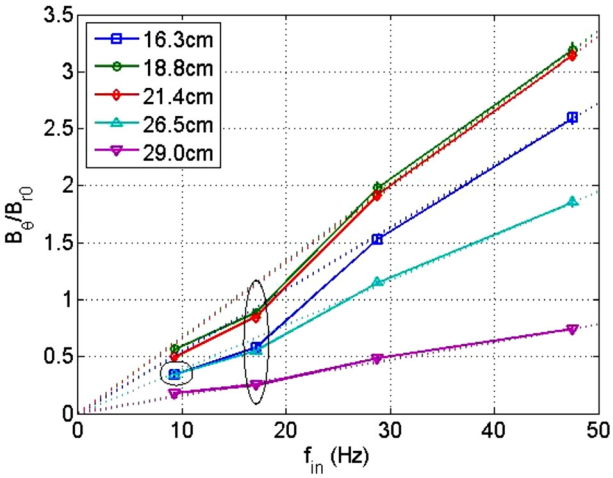

FIG. 4. ω-gain B_θ/B_{r0} for increasing inner cylinder rotation rate. Square markers are measured ω-gain at 5 radii (R = 16.3, 18.8, 21.4, 26.5, and 29.0 cm, respectively). Dotted lines are a linear fit to the largest measured gain for each location. Note that the errors are less than 7% so the error bars are about the symbol size. Also note that the data points fall roughly on the dotted lines if encircled points are removed.

The pressure sensors confirm the observations made with the magnetic sensors. Fig. 6(b) shows peaks at the identical frequency ratios to Fig. 6(a). The peak is quite prominent at 9.3 Hz, appears at reduced power at 17.1 Hz, and vanishes at higher rotation rates. Once again, this is observed on all pressure sensors on the end-plate at their 7 different radial positions.

The peaks in the power spectra at low inner cylinder rotation speeds hint at a relatively coherent flow pattern on top of a turbulent background flow. The decrease of magnitude and eventual disappearance of the peaks suggest that the correlation length of the fluctuations may be changing with rotation rate. The large low-frequency peak may be due to large-scale coherent motions with large correlation length. If this is the case, it can explain why we see the transition in the gain measurements in Fig. 5 between $f_{in} = 17.1$ Hz and $f_{in} = 28.8$ Hz.

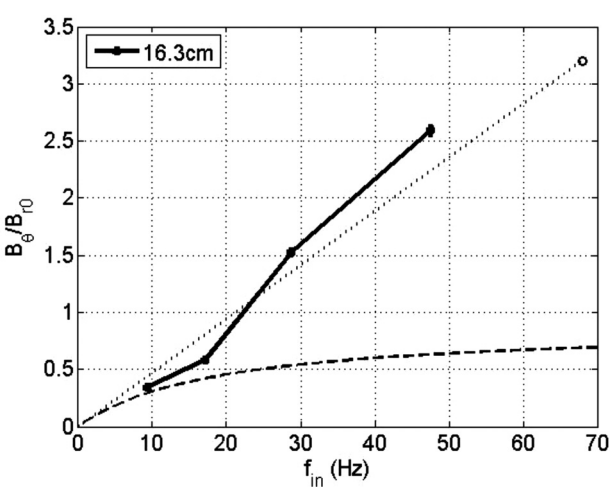

FIG. 5. ω-Gain B_θ/B_{r0} vs Rm at R = 16.3 cm. The dotted line shows the anticipated gain based on scaling the previously measured gain in stable Taylor-Couette flow and assuming no effective turbulent enhancement to the resistivity. The dashed line is plotted according to Eq. (18) with κ determined from torque measurements with water showing the expected saturation level for turbulence with a correlation length of ΔR.

Yet another view of the same phenomenon is shown in Fig. 6(c). If the coherence length of the velocity fluctuations is changing, it should also result in a change in the correlation time of the magnetic fluctuations. At $f_{in} = 9.3$ Hz, the auto-correlation curve of B_θ is like that of a damped sine wave. If one measures the time between two consecutive peaks of B_θ, one finds the period is $T \approx \Delta t = 0.37\,\mathrm{s} = 1/0.29 f_{in}$, consistent with the most prominent peak in Fig. 6(a). B_z is also like a damped sine wave with $T \approx 0.35$ s, but its auto-correlation curve decays more rapidly than that of B_θ. Compared with B_θ and B_z, the B_r auto-correlation curve decays more rapidly. Although we still can see a peak in B_r at around 0.2 s (at $f_{in} = 9.3$ Hz), its auto-covariance is 0.14. At $f_{in} = 17.1$ Hz, we see the auto-covariance of B_θ decays more rapidly than the case at $f_{in} = 9.3$ Hz. For B_r and B_z, the periodic behavior is almost gone. At $f_{in} = 28.8$ and 48.6 Hz, there is no obvious periodic behavior and the correlation times have become very short.

The observations in the fluctuation spectra are consistent with a decreasing correlation length as inner cylinder rotation increases. This could explain why there is no enhanced resistivity observed at higher rotation rates.

D. Penetration time measurement

The observed effect of $\eta_\perp^{turb}$ through the penetration method shows that $\eta_\perp^{turb}$ is one order of magnitude smaller than the estimated η^{turb} by the homogenous isotropic approximation at all the rotation rates.

Figs. 7(a) and 7(b) show the fall time of B_z at $r = 19.6$ cm with the apparatus rotating at $f_{in} = 17.1$ Hz and 47.6 Hz (corresponding to Rm = 31 and 87 in Fig. 4). To facilitate the comparison of fall times with/without the inner cylinder rotating, the signals are all normalized. To improve signal to noise, the magnetic field was pulsed multiple times at each rotation rate and the $B_z(t)$ data averaged over several pulses. On the left, the green curves are the coil current, which fall much faster than the magnetic signals. The blue curves are B_z averaged over 3 (Fig. 7(a)) and 4 (Fig. 7(b)) pulses and measured with the inner-cylinder rotating. The red curves are B_z taken with the inner cylinder stationary. One cannot perceive any difference in the fall time between the rotating and stationary measurements.

According to Eq. (17), the homogeneous and isotropic approximation gives turbulent resistivity of about $0.7\eta_{Na}$ and $2\eta_{Na}$ at $f_{in} = 17.1$ Hz and 47.6 Hz. The region of data inside the dashed black boxes is expanded in the right panels of Fig. 7. To the top right panel ($f_{in} = 17.1$ Hz) we added dotted cyan curves showing how the B_z time decay would appear if $\eta_\perp^{turb}$ were 70% of η_{Na} and also dotted black curves demonstrating the effect of a 20% turbulent resistivity enhancement. Clearly, our measurements show that the resistivity enhancement is not 70% nor is it even 20%. Similarly, to the bottom right panel we added cyan and black curves to demonstrate that at 47.6 Hz, there is obviously neither a 200% enhancement nor is there even a 20% enhancement of the turbulent resistivity.

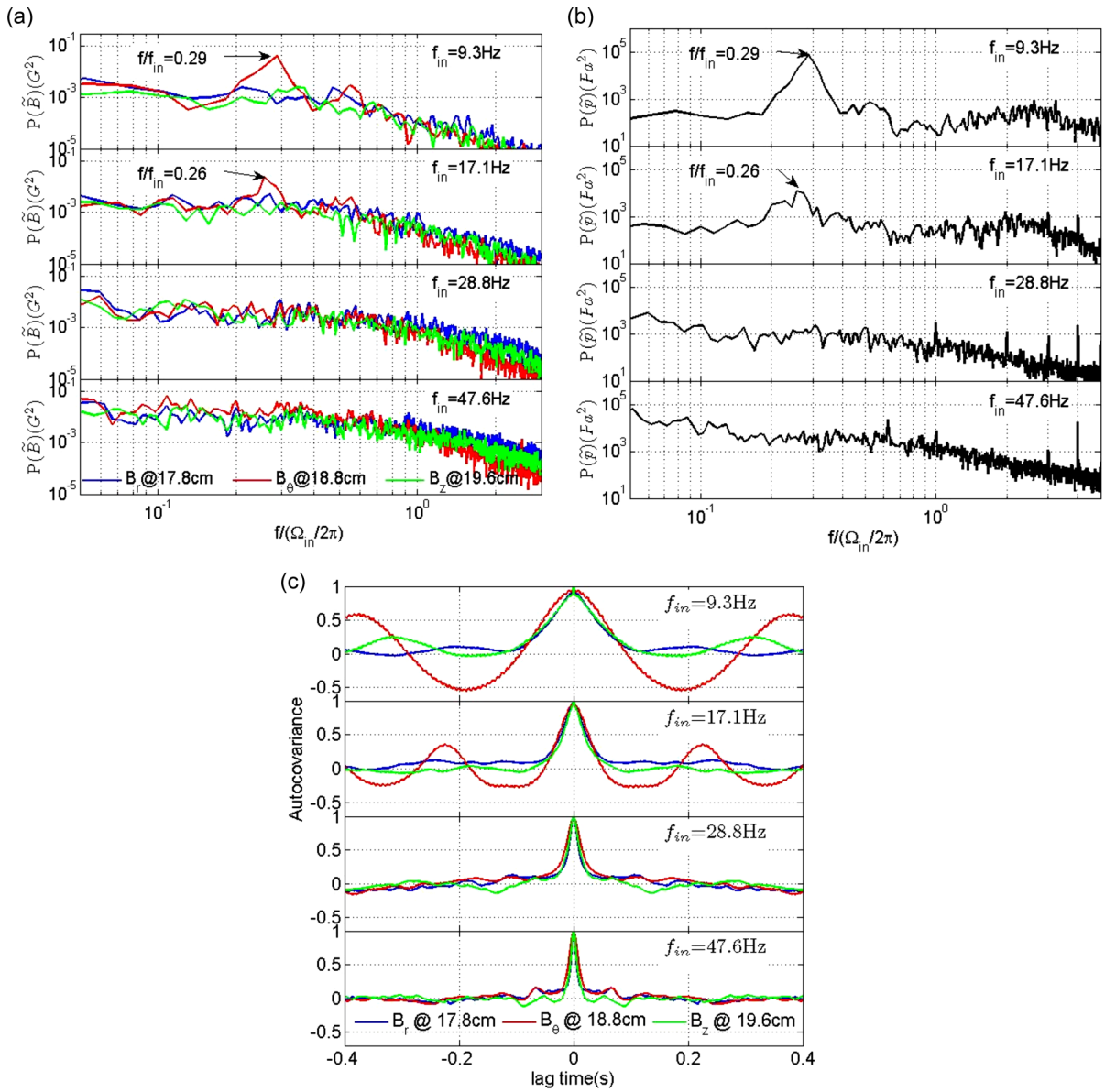

FIG. 6. Analysis of magnetic field and pressure fluctuations. (a) Spectra of $\widetilde{\mathbf{B}}$ measured from Hall-effect sensors. The three components are measured at nearby locations: B_r at 17.8 cm, B_θ at 18.8 cm and B_z at 19.6 cm. (b) Spectra of $\widetilde{p}$ measured at a radius of 26.7 cm. (c) Auto-covariance of B_r at 17.8 cm, B_θ at 18.8 cm and B_z at 19.6 cm. The external field is quadrupole. The spectra and auto-covariance curves are the results of averaging over at least 20 time segments.

Having clearly shown that the turbulent resistivity is far less than predicted by Eq. (17), one can now fit the measured data to quantify how much turbulent resistivity may be present. The results of this fit are presented in Figure 8. In the following, we explain, in detail, how we arrived at this result.

Not surprisingly, the measured decay curves are pure exponential functions $B = B_0 e^{-t/\tau_0}$ (note $\frac{\eta}{\mu_0}\frac{k_n^2}{R_0^2}$'s in Eq. (16) are different for different k_n's). However, the magnetic field decay curve in our apparatus is still a function of $\eta_{\text{eff}} t$ for a given location, or

$$\langle B_z(t)\rangle = f(\eta_{\text{eff}} t),$$

where $\eta_{\text{eff}} = \eta_{\text{Na}} + \bar{\eta}_\perp^{\text{turb}}$ is the effective resistivity (as discussed in Section III, decay time is mostly affected by $\eta_\perp^{\text{turb}}$), the overbar on $\eta_\perp^{\text{turb}}$ indicates the value is a mean value from the outer radius to the location of the sensor, and $\langle\rangle$ represents an ensemble average. Ideally, since the decay curve without rotation is

$$F(t) = f(\eta_{Na} t),$$

while the curve with rotation is

$$G(t) = f(\eta_{\text{eff}} t),$$

it should happen that $F[(1+R_\eta)t] = G(t)$, where $R_\eta = \bar{\eta}_\perp^{\text{turb}}/\eta_{\text{Na}}$.

In practice, by comparing the decay curves with and without the inner cylinder rotating, we calculated R_η by finding an R_η such that the least squares in a time period $[0, t_0]$

$$\|F[(1+R_\eta)t] - G(t)\|_2^2 \text{ in } [0, t_0]$$

is minimized. The fluctuation component in the decay curves can cause errors. This error can be estimated by varying t_0.

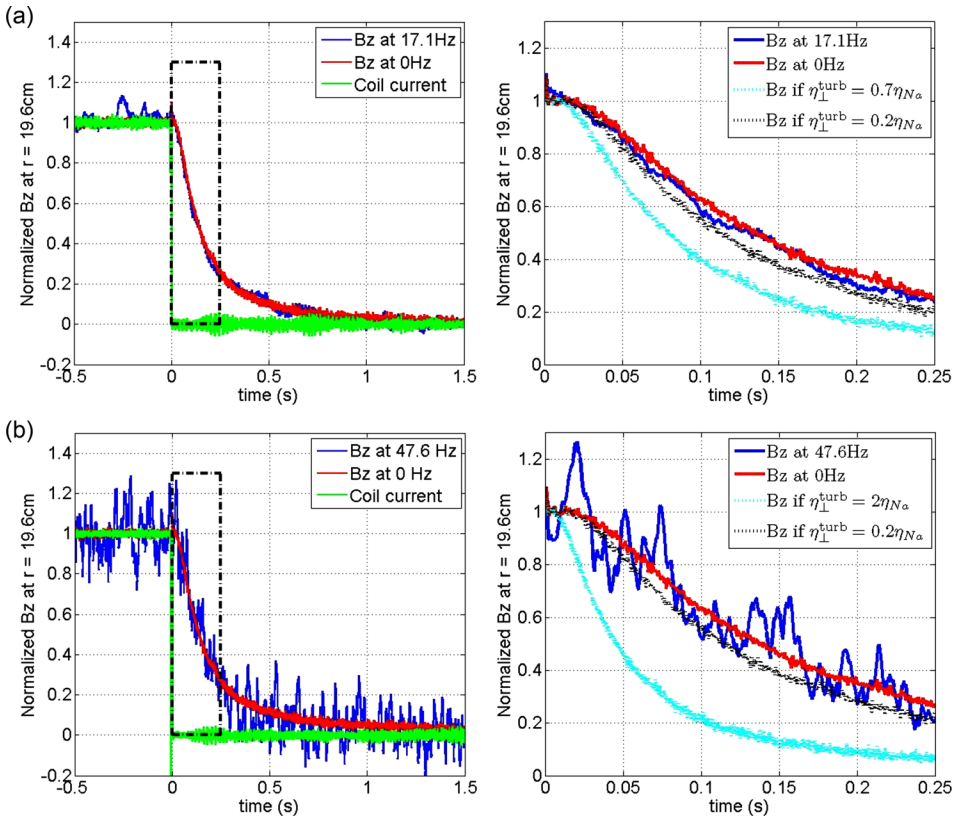

FIG. 7. In the left, the blue and red curves are $B_z(r = 19.6\,\text{cm})$ delay curves for (a) $\Omega_{\text{in}}/2\pi = 17.1\,\text{Hz}$ (Rm = 31) (b) $\Omega_{\text{in}}/2\pi = 47.6\,\text{Hz}$ (Rm = 86), and $\Omega_{outer} = 0$ Hz. The curves with rotation are averaged by 3 (Fig. 7(a)) and 4 (Fig. 7(b)) measured curves to reduce the fluctuation level. One can see the decay time of the coil current (the green curve) is much shorter than the decay time of Bz so that its effect on the overall decay time is insignificant. The portion in the box with black dashed lines is zoomed in the right. According to Eq. (17), the homogeneous and isotropic approximation gives about $0.7\eta_{Na}$ and $2\eta_{Na}$ at 17.1 Hz and 47.6 Hz, respectively. To show how the B_z would decay according to Eq. (17), for 17.1 Hz, $B_z(r = 19.6\,\text{cm})$ curves with time scale compressed by a factor $\frac{1}{1+0.7} \approx 0.588$ is plotted by cyan dots; for 47.6 Hz, a dotted cyan curve with a factor $\frac{1}{1+2} \approx 0.333$ is plotted. B_z with a factor of $\frac{1}{1+0.2} \approx 0.833$ is also plotted by black dots for both rotation rates to show that even if $\eta_\perp^{\text{turb}}/\eta_{Na} = 0.2$, B_z should decay faster than the observed decay rate. The external magnetic field is dipole.

By varying t_0 from 0.5 to 1.5 s, we calculate the R_η's, as shown in Fig. 8. They are only a few percent of the resistivity of sodium at all rotation rates.

E. Discussion

We have read with interest an experimental report of a negative β-effect by a dynamo group at Grenoble.[44] In contrast, both the methods used in our experiment resulted in a negligible β-effect. More specifically, the observations using both the azimuthal wind-up of an applied magnetic field and pulsed decaying magnetic fields show that the inductive response of hydrodynamically unstable rotating shear flow is described well by the mean flow profile without recourse to additional transport from correlated fluctuations. One possible explanation for this outcome may be shear suppression of the large-scale velocity fluctuations.

Flow shear can speed up the turbulent de-correlation.[45] In the homogeneous isotropic turbulence approximation, we assume the size of the largest eddies is $\sim\Delta R$. However, a necessary condition for this approximation to be valid is that the velocity gradient of eddies of a certain scale must at least be bigger than the velocity gradient of the background mean field. The specific angular momentum in the bulk is approximately $\bar{L}_\theta = \Omega_{\text{in}} R_{\text{in}}^2/2$, so the velocity gradient is around

$$\text{Grad}_{mean} \approx \Delta U/\Delta R \approx \bar{L}_\theta(1/R_{\text{in}} - 1/R_{\text{out}})/\Delta R.$$

For $\Omega_{\text{in}} = 47.6\text{Hz}$, $\text{Grad}_{mean} \approx 75\,\text{s}^{-1}$. From Eqs. (10) and (17), we get

$$\tilde{u} = \frac{3}{\mu_0 \Delta R}\kappa \text{Re}.$$

At $\Omega_{\text{in}} = 47.6\text{Hz}$, Re is $\sim 10^7$ for sodium at 110 °C. We get $\tilde{u} = 3.2\,\text{m/s}$.

$$\text{Grad}_{fluct} = \tilde{u}/\Delta R \approx 21\,\text{s}^{-1} < \frac{1}{3}\text{Grad}_{mean}.$$

Note that both Grad_{mean} and Grad_{fluct} are $\propto$ Re. Hence, $\text{Grad}_{mean} > \text{Grad}_{fluct}$ for all rotation rates studied. Thus, it is not valid to assume the size of the largest eddies is $\sim\Delta R$. The real correlation length should be reduced by strong flow shear, as discussed by Terry.[45]

V. SUMMARY

Both steady-state measurements of the azimuthal wind-up of an applied magnetic field by differential rotation and

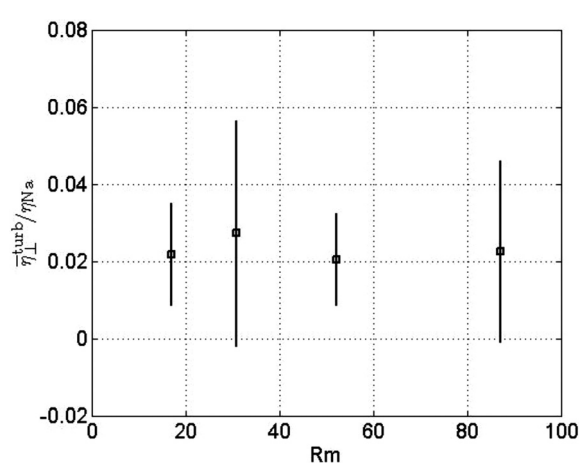

FIG. 8. $\bar{\eta}_\perp^{\text{turb}}/\eta_{\text{Na}}$ vs Rm at R = 19.6 cm.

measurements of the decay time of a pulsed magnetic field show that there is no significant turbulent resistivity observed in a hydrodynamically unstable Taylor-Couette flow of liquid sodium. The mean induction of the flow is described entirely by the mean flow profile. Residual coherent fluctuations at lower rotation rates may cause some reduction in magnetic flux transport, but the flow undergoes a transition to fluctuations with very short correlation times.

To confirm our conjecture that velocity shear is increasing the turbulent decorrelation rate, direct velocity measurement is necessary. Unfortunately, such measurements are currently not available. A velocity probe based on the same principle as one in Wisconsin[27,46] is being considered for future upgrading.

ACKNOWLEDGMENTS

We gratefully acknowledge the funding over the years by NSF (Grant No. 1102444), and LANL via a cooperative arrangement with NM-Tech. We offer heartfelt thanks to National Instruments for providing much of the data acquisition system. S.A.C. and H.L. also acknowledge the support by the LANL/LDRD program and DoE/OFES through CMSO. J.S. expresses thanks to the New Mexico Tech office of R&ED for bridging funds between grants. Several members of the Colgate family and other private investors have contributed funds and we are deeply appreciative of their commitment to this project. M.D.N. acknowledges the support from CMSO PHY 08-21899 covering his time for this project.

APPENDIX: DECAY TIME FOR A SIMPLE MODEL

To estimate the decay time, we consider an infinitely long cylinder with effective resistivity η_{eff} and radius R. The external magnetic field has only axial component $\vec{B} = B(t)\hat{z}$, and

$$B(t) = \begin{cases} B_0 & t < 0 \\ 0 & t \geq 0. \end{cases}$$

In this simplified model, the only nontrivial component is B_z. So, as discussed in Sec. III B

$$\frac{\partial \overline{B_z}}{\partial t} = \frac{\eta_{\text{eff}}}{\mu_0} \nabla^2 \overline{B_z}, \tag{A1}$$

where $\eta_{\text{eff}} = \eta + \eta_{\perp}^{\text{turb}}$. Since $\partial/\partial\theta \to 0$ and $\partial/\partial z \to 0$, Eq. (A1) becomes

$$\frac{\partial \overline{B_z}}{\partial t} = \frac{\eta_{\text{eff}}}{\mu_0} \frac{1}{r} \frac{\partial}{\partial r}\left(r \frac{\partial \overline{B_z}}{\partial r}\right), \tag{A2}$$

with

$$\overline{B_z}(0, r) = B_0, \quad 0 \leq r < R_0,$$

and

$$\overline{B_z}(t, R_0) = 0 \quad t \geq 0.$$

One way to solve the problem is to use the separation of variables method. By assuming, the solution is of the form $\overline{B_z}(t, z) = T(t)R(r)$, from Eq. (A2), we can obtain

$$\frac{\mu_0}{\eta_{\text{eff}}} \frac{\frac{\partial T}{\partial t}}{T} = \frac{\frac{1}{r}\frac{\partial}{\partial r}\left(r \frac{\partial R}{\partial r}\right)}{R} = -\frac{k^2}{R_0^2}. \tag{A3}$$

In Eq. (A3), k must be real to satisfy the conditions. The solutions of

$$\frac{\frac{1}{r}\frac{\partial}{\partial r}\left(r \frac{\partial R}{\partial r}\right)}{R} = -\frac{k^2}{R_0^2}$$

are $R(r) = J_0(kr/R_0)$, where J_0 is the Bessel function of the first kind and zeroth order. The boundary condition of $R(R_0) = 0$ requires $J_0(k) = 0$, which yields infinite number of constant k_n. For each k_n

$$\frac{\partial T}{\partial t} = -\frac{\eta_{\text{eff}}}{\mu_0} \frac{k_n^2}{R_0^2} T,$$

which has the solution

$$T(t) = A_n e^{-\frac{\eta_{\text{eff}} k_n^2}{\mu_0 R_0^2} t}.$$

Therefore, the solution is

$$\overline{B_z}(t, r) = \sum_{n=1}^{\infty} A_n J_0(k_n r/R_0) e^{-\frac{\eta_{\text{eff}} k_n^2}{\mu_0 R_0^2} t}. \tag{A4}$$

From the initial condition that

$$\overline{B_z}(0, r) = B_0 = \sum_{n=1}^{\infty} A_n J_0(k_n r/R_0), \text{ for } r < R_0,$$

we can get

$$A_n = \frac{2B_0}{k_n J_1(k_n)}. \tag{A5}$$

So the final solution is

$$\overline{B_z}(t, r) = \sum_{n=1}^{\infty} \frac{2B_0}{k_n J_1(k_n)} J_0(k_n r/R_0) e^{-\frac{\eta_{\text{eff}} k_n^2}{\mu_0 R_0^2} t}. \tag{A6}$$

Given the outer cylinder radius, conductivity of sodium, and assuming the lowest wavenumber radial wavefunction with $k_0 = 2.4$, we obtain a decay time of about 200 ms.

[1]M. Kono and P. H. Roberts, Rev. Geophys. **40**, 4-1, doi:10.1029/2000RG000102 (2002).
[2]P. Charbonneau, *Solar and Stellar Dynamos* (Springer, Verlag, 2013).
[3]A. G. Lyne and F. Graham-Smith, *Pulsar Astronomy*, 3rd ed. (Cambridge University Press, 2006).
[4]J. Frank, A. King, and D. Raine, *Accretion Power in Astrophysics*, 3rd ed. (Cambridge University Press, 2002).
[5]A. Gailitis, O. Lielausis, S. Dement'ev, E. Platacis, A. Cifersons, G. Gerbeth, T. Gundrum, F. Stefani, M. Christen, H. Hänel, and G. Will, Phys. Rev. Lett. **84**, 4365 (2000).

[6]A. Gailitis, O. Lielausis, E. Platacis, S. Dement'ev, A. Cifersons, G. Gerbeth, T. Gundrum, F. Stefani, M. Christen, and G. Will, Phys. Rev. Lett. **86**, 3024 (2001).
[7]A. Gailitis, O. Lielausis, E. Platacis, G. Gerbeth, and F. Stefani, Rev. Mod. Phys. **74**, 973 (2002).
[8]A. Gailitis, O. Lielausis, E. Platacis, G. Gerbeth, and F. Stefani, Phys. Plasmas **11**, 2838 (2004).
[9]R. Stieglitz and U. Müller, Phys. Fluids **13**, 561 (2001).
[10]U. Müller, R. Stieglitz, and S. Horany, J. Fluid Mech. **498**, 31 (2004).
[11]F. Ravelet, M. Berhanu, R. Monchaux, S. Aumaître, A. Chiffaudel, F. Daviaud, B. Dubrulle, M. Bourgoin, P. Odier, N. Plihon, J.-F. Pinton, R. Volk, S. Fauve, N. Mordant, and F. Pétrélis, Phys. Rev. Lett. **101**, 074502 (2008).
[12]M. Berhanu, G. Verhille, J. Boisson, B. Gallet, C. Gissinger, S. Fauve, N. Mordant, F. Pétrélis, M. Bourgoin, P. Odier, J.-F. Pinton, N. Plihon, S. Aumaître, A. Chiffaudel, F. Daviaud, B. Dubrulle, and C. Pirat, Eur. Phys. J. B **77**, 459 (2010).
[13]G. Verhille, N. Plihon, M. Bourgoin, P. Odier, and J.-F. Pinton, New J. Phys. **12**, 033006 (2010).
[14]S. A. Colgate, H. Li, and V. Pariev, Phys. Plasmas **8**, 2425 (2001).
[15]S. A. Colgate, V. I. Pariev, H. F. Beckley, R. Ferrel, V. D. Romero, and J. C. Weatherall, Magnetohydrodynamics **38**, 129 (2002).
[16]H. F. Beckley, S. A. Colgate, V. D. Romero, and R. Ferrel, Astrophys. J. **599**, 702 (2003).
[17]V. I. Pariev and S. A. Colgate, Astrophys. J. **658**, 114 (2007).
[18]V. I. Pariev, S. A. Colgate, and J. M. Finn, Astrophys. J. **658**, 129 (2007).
[19]S. A. Colgate, H. Beckley, J. Si, J. Martinic, D. Westpfahl, J. Slutz, C. Westrom, B. Klein, P. Schendel, C. Scharle, T. McKinney, R. Ginanni, I. Bentley, T. Mickey, R. Ferrel, H. Li, V. Pariev, and J. Finn, Phys. Rev. Lett. **106**, 175003 (2011).
[20]F. Krause and K.-H. Rädler, *Mean-Field Magnetohydrodynamics and Dynamo Theory* (Pergamon Press, 1980).
[21]K.-H. Rädler, in *Magnetohydrodynamics, Fluid Mechanics and its Applications* Vol. 80, edited by S. S. Molokov, R. Moreau, and H. K. Moffatt (Springer, Netherlands, 2007), pp. 55–72.
[22]C. Jones, in *Dynamos, Volume LXXXVIII: Lecture Notes of the Les Houches Summer School 2007*, edited by P. Cardin and L. Cugliandolo (Elsevier Science, 2008), pp. 45–136.
[23]L. L. Kitchatinov, V. V. Pipin, and G. Rüdiger, Astron. Nachr. **315**, 157 (1994).
[24]A. B. Reighard and M. R. Brown, Phys. Rev. Lett. **86**, 2794 (2001).
[25]P. Frick, V. Noskov, S. Denisov, and R. Stepanov, Phys. Rev. Lett. **105**, 184502 (2010).
[26]M. D. Nornberg, E. J. Spence, R. D. Kendrick, C. M. Jacobson, and C. B. Forest, Phys. Plasmas **13**, 055901 (2006).
[27]K. Rahbarnia, B. P. Brown, M. M. Clark, E. J. Kaplan, M. D. Nornberg, A. M. Rasmus, N. Z. Taylor, C. B. Forest, F. Jenko, A. Limone, J.-F. Pinton, N. Plihon, and G. Verhille, Astrophys. J. **759**, 80 (2012).
[28]H. F. Beckley, "Measurements of annular Couette flow stability at the fluid Reynolds number $\mathrm{Re} = 4.4\times10^6$: The fluid dynamic precursor to a liquid sodium $\alpha\omega$ dynamo," Ph.D. dissertation (New Mexico Institute of Mining and Technology, 2002).
[29]J. Si, S. A. Colgate, H. Li, J. Martinic, and D. Westpfahl, Rev. Sci. Instrum. **84**, 104501 (2013).
[30]L. Landau and E. M. Lifshitz, *Fluid Mechanics: Course of Theoretical Physics*, 2nd ed. (Butterworth-Heinemann Ltd., 1987), Vol. 6.
[31]D. S. Zimmerman, S. A. Triana, H.-C. Nataf, and D. P. Lathrop, J. Geophys. Res. Solid Earth **119**, 4538 (2014).
[32]G. I. Taylor, Philos. Trans. R. Soc., A **223**, 289 (1923).
[33]G. P. Smith and A. A. Townsend, J. Fluid Mech. **123**, 187 (1982).
[34]D. P. Lathrop, J. Fineberg, and H. L. Swinney, Phys. Rev. Lett. **68**, 1515 (1992).
[35]D. Lathrop, J. Fineberg, and H. Swinney, Phys. Rev. A **46**, 6390 (1992).
[36]G. S. Lewis and H. L. Swinney, Phys. Rev. E **59**, 5457 (1999).
[37]T. T. Lim and K. S. Tan, Phys. Fluids **16**, 140 (2004).
[38]B. Dubrulle, O. Dauchot, F. Daviaud, P.-Y. Longaretti, D. Richard, and J.-P. Zahn, Phys. Fluids **17**, 095103 (2005).
[39]B. Eckhardt, S. Grossmann, and D. Lohse, J. Fluid Mech. **581**, 221 (2007).
[40]M. Burin, E. Schartman, and H. Ji, Exp. Fluids **48**, 763 (2010).
[41]H. J. Brauckmann and B. Eckhardt, J. Fluid Mech. **718**, 398 (2013).
[42]U. Frisch, *Turbulence: The Legacy of A. N. Kolmogorov* (Cambridge University Press, 1995).
[43]C. R. Doering and P. Constantin, Phys. Rev. Lett. **69**, 1648 (1992).
[44]S. Cabanes, N. Schaeffer, and H.-C. Nataf, Phys. Rev. Lett. **113**, 184501 (2014).
[45]P. W. Terry, Rev. Mod. Phys. **72**, 109 (2000).
[46]R. Ricou and C. Vives, Int. J. Heat Mass Transfer **25**, 1579 (1982).